Journal of Biomechanics 85 (2019) 118–125

Contents lists available at ScienceDirect

Journal of Biomechanics

journal homepage: www.elsevier.com/locate/jbiomech
www.JBiomech.com

A coupled framework of *in situ* and *in silico* analysis reveals the role of lateral force transmission in force production in volumetric muscle loss injuries

Amanda M. Westman [a], Sarah E. Dyer [a], J. David Remer [a], Xiao Hu [a], George J. Christ [a,b,*], Silvia S. Blemker [a,b,c,d,*]

[a] Biomedical Engineering, University of Virginia, Charlottesville, VA, United States
[b] Orthopaedic Surgery, University of Virginia, Charlottesville, VA, United States
[c] Mechanical and Aerospace Engineering, University of Virginia, Charlottesville, VA, United States
[d] Ophthalmology, University of Virginia, Charlottesville, VA, United States

ARTICLE INFO

Article history:
Accepted 10 January 2019

Keywords:
Finite-element modeling
Tissue engineering
Volumetric muscle loss
Muscle mechanics
Lateral force transmission

ABSTRACT

Volumetric muscle loss injuries (VML) are challenging to treat because of the variability in wound location. Regenerative medicine offers promising alternative treatments, but there is little understanding of the correlation between magnitude of VML injuries and corresponding functional deficits that must be addressed. There is a need for a tool that can elucidate the relationship between VML injury and force loss, as well as the impact on specific mechanisms responsible for force production. The purpose of this study was to develop a novel coupled framework of *in situ* and *in silico* methods to more precisely understand the relationship between injury location and force production deficits. We created a three-dimensional finite-element model of the pennate latissimus dorsi (LD) muscle in the rat and validated the model experimentally. We found that the model's prediction (2.6 N/g Model I, 2.1 N/g Model V) compared favorably to *in situ* testing of isometric force generation of the injured rat LD muscle (2.8 ± 0.3 N/g Experimental I, 2.0 ± 0.2 N/g Experimental V). Further model analysis revealed that the contribution from lateral and longitudinal force transmission to the total force varied with injury location and led to a greater understanding of the mechanisms responsible for VML-related force deficits. In the future, the coupled computational and experimental framework can be used to inform development of preclinical VML injury models that better recapitulate the spectrum of VML injuries observed in affected patients, and the mechanistic insight can accelerate the creation of improved regenerative therapeutics for VML injuries.

1. Introduction

Volumetric muscle loss (VML) injuries result in a permanent loss of muscle structure and function. These types of deficits can result from congenital diseases and are also common after trauma, including combat-related wounds. Development of technologies to treat VML injuries is hampered by the fact that the spectrum of injuries and wound locations vary widely (Corona et al., 2015). Regenerative medicine is a promising approach for the treatment of these injuries that has the potential to address the complexity of VML wounds; however, within the literature, a wide variety of *in vivo* models are currently used to study these injuries — making straightforward comparisons of the efficacy of distinct technologies challenging. Most commonly, VML injuries have been studied in limb muscles of rodents (Baker et al., 2017; Corona et al., 2013; Passipieri et al., 2017; Quarta et al., 2017). These studies utilize injuries that differ in location; therefore, the measured magnitudes of corresponding functional deficits vary widely. Taken together, these observations reinforce the importance of improved understanding of the mechanisms responsible for VML-induced force deficits. The focus of this study is to systematically characterize the impact of injury location on the biomechanics of force production in intact and VML-injured muscles in the rat latissimus dorsi (LD) muscle—a pennate muscle that is clinically relevant and

---

* Corresponding authors at: University of Virginia, Box 800759, Charlottesville, VA 22903, United States.

E-mail addresses: gjc8w@eservices.virginia.edu (G.J. Christ), ssb6n@eservices.virginia.edu (S.S. Blemker).

https://doi.org/10.1016/j.jbiomech.2019.01.025
0021-9290/© 2019 Published by Elsevier Ltd.

dimensionally similar to human craniofacial muscles that are affected by VML injuries (Christ et al., 2015).

In this regard, force production within skeletal muscle is dependent on both the active and passive muscle fiber characteristics and the intramuscular connective tissue properties (Street, 1983; Zajac, 1989). In the case of VML injuries, the direct connection of myofibers to the tendon is disrupted which dramatically impairs the ability of the fibers to transmit force longitudinally. Previous studies have shown that skeletal muscle fibers without direct myotendinous connections have the potential to contribute to force production within a muscle by transmitting force laterally through the connective tissue (Huijing et al., 1998; Jaspers et al., 1999; Street, 1983). It stands to reason, therefore, that lateral force transmission contributes to force production in VML injuries. However, it remains unclear how injury location affects the contribution of lateral force transmission to whole muscle force production.

In silico three-dimensional finite-element (FE) modeling provides a framework for determining the complex relationship between injury location and force production in VML injuries. FE skeletal muscle models incorporate muscle geometry, fiber architecture, shear properties, volume preservation, and active and passive muscle fiber characteristics to create a tool which can be used to explore and analyze the mechanisms of muscle function (Blemker et al., 2005). For example, a number of human skeletal whole muscle models have been developed to: (1) determine the force production of individual muscles at varying locations within the pelvic floor (Martins et al., 2007), (2) evaluate stretch and strain changes during contraction of the biceps brachii and biceps femoris longhead (Blemker et al., 2005; Rehorn and Blemker, 2010), and (3) assess the effects of muscle activation in cleft palate repair (J.M. Inouye et al., 2015). Additionally, an FE model with simplified muscle structure has been used to study the mechanics of force transmission between extracellular matrix and myofiber (Yucesoy et al., 2003, 2002). However, to our knowledge, there are no published reports using FE skeletal muscle modeling to improve mechanistic understanding of how VML injury location affects the corresponding functional deficits.

Our goal, therefore, was to develop a coupled framework of *in situ* and *in silico* methods to uncover the relationship between VML injury location and muscle force production. The *in silico* models allow us to optimize experimental variables, such as injury location, and better design experiments prior to expensive *in vivo* testing. This report focused on using the capabilities of the model in a manner that extends beyond experimental analysis to explore how VML injury can alter the contributions of lateral and longitudinal force transmission. As a first step in this direction, we created FE models of five distinct rat LD VML injuries, validated the predicted force deficit experimentally in two of these injuries, and then used the analytic capabilities of the model to identify and compare the biomechanical mechanisms governing force production/force loss among the distinct injury locations.

2. Methods

2.1. Finite-element model

The three-dimensional FE model of an intact rat LD was created based on measurements from dissected LDs of four male Lewis rats (Passipieri et., al 2019). The x-y dimensions and weight of the LDs were measured, and the thickness was measured at 12 locations around the LDs. Three-dimensional model of the LD was simplified to have a shape that combines one rectangle and one triangle medial in the x-y plane with varying thickness in the z-direction (Fig. 1A model compared to Fig. 4C explanted intact muscle). The FE model was meshed using 4-node enhanced tetrahedral elements (4149 elements) in AMPS finite-element software (AMPS Technologies).

2.1.1. Muscle model

Skeletal muscle properties were implemented using a constitutive relationship that has previously been described in detail (Blemker et al., 2005). The LD was modeled as a transversely isotropic, hyperelastic and quasi-incompressible material with a preferred direction. Muscle fiber direction originates along the spine and runs to the insertion at the humerus (Fig. 1A). Fiber trajectories were determined using computational fluid dynamics and then each element of the model was assigned a fiber direction (Fig. 1A) (Handsfield et al., 2017; J. Inouye et al., 2015). The model's along-fiber stretch captures the longitudinal force development and transmission in the same direction using active (Zajac, 1989) and passive stress-strain relationships (Blemker et al., 2005). Model fiber stretch is defined as $\lambda = l/L_0$ ($\lambda < 1$ for a shortening fiber), l is the final fiber length, and L_0 is the initial fiber length and assumed to be at optimal length. The model's shearing along and across the fiber direction is representative of lateral force transmission between fibers via the extracellular matrix.

The intact LD muscle model was calibrated to fit intact experimental data of isometric force. The LD thickness varies across its length and width making it challenging to calculate the true cross-sectional area and thus determine the peak isometric stress (σ_{max}) of the rat LD. A sensitivity analysis of the σ_{max} parameter was run (Fig. 1B), model force outputs were compared to intact experimental data, and 1.4×10^5 Pa was the parameter value which best replicated an *in situ* LD muscle (Fig. 1C). The final model parameter values used in this study for both intact and injured models are in Table 1.

2.1.2. Model simulations

To replicate *in situ* experimental testing conditions, the cranial rectangular surface and caudal rectangular and triangular edges of the model were fixed. In total, five different injuries (11×15 mm^2 and entire thickness of the muscle) were created at various locations within the muscle model (Fig. 2) and isometric contractions were simulated (Strain-Enriched FEA, AMPS Technologies). First, an injury was created in the middle of the rectangular portion of the LD (Model I) and then the injury was moved within the boundaries of the muscle and below the thoracodorsal motor nerve (Model II – V). It would not be possible to stimulate the LD using *in situ* testing if an injury removed the motor nerve innervation. Muscle activation levels were set at the maximum activation for all trials to simulate maximum tetanic force. Total force of the modeled LD was measured in the y-direction on the cranial rectangular surface in the x-z plane. A mesh sensitivity analysis of the intact LD model demonstrated that a consistent force value is achieved with meshes greater than 2000 elements. Injury model mesh counts were all above this minimum value, providing confidence in the output force of these models.

2.1.3. Model analysis

To directly compare model predictions and experimental measurements, the model force prediction was normalized to LD model weight. The model is a simplified geometry of the LD muscle and likely overestimates the true volume of the LD, thus the rat LD model assumed mass per unit volume was calculated by dividing the average weight of intact experimental LDs (Table 2) by the intact muscle model volume. Then the weights of Models I (1.570 g) and V (1.521 g) were determined using the model volumes and calculated rat LD model assumed mass per unit volume.

To determine force generation for the end-to-end fibers region of the muscle, MATLAB was used to identify the nodes on the

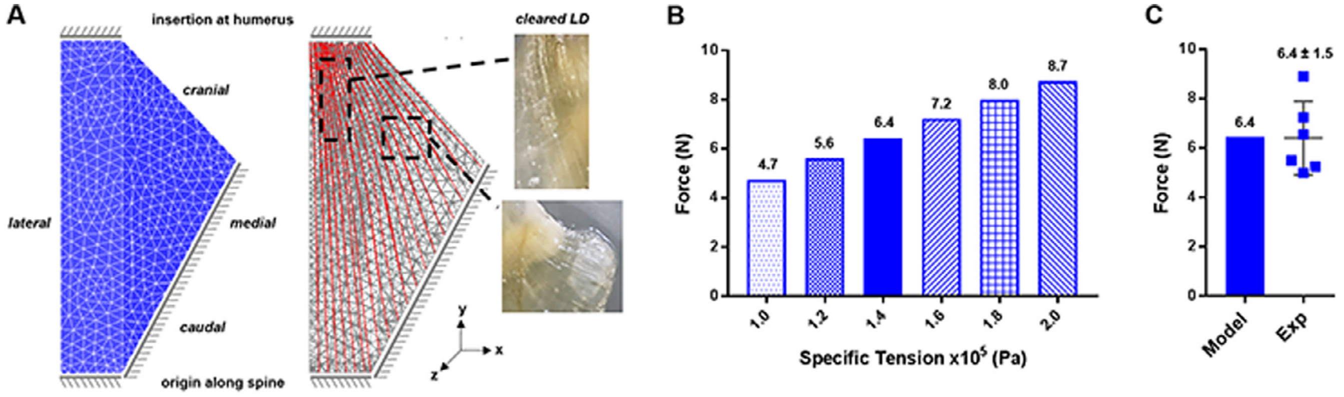

Fig. 1. Three-dimensional finite element model of the rat latissimus dorsi (LD) constrained as shown along the cranial rectangular edge and caudal rectangular and triangular edges with the elements (A, left). The model fiber trajectories highlighted (A, middle) are similar to the observed fiber directions of a cleared LD muscle (A, right). Sensitivity analysis of specific tension parameter to determine ideal parameter value (B). Intact LD model was calibrated to intact experimental data (n = 6), and specific tension of 1.4×10^5 Pa best replicated experimental isometric force measurements of intact LDs (C).

Table 1
Material parameters for the LD muscle model (Blemker et al., 2005). Passive parameters (P_1, P_2, λ^*) were determined experimentally (Passipieri et., al 2019).

σ_{max}	P_1	P_2	λ^*	G_1	G_2	K
Pa	dimensionless			Pa	Pa	Pa
1.4×10^5	0.0043	14.2395	1.3306	3870	22,400	1×10^7

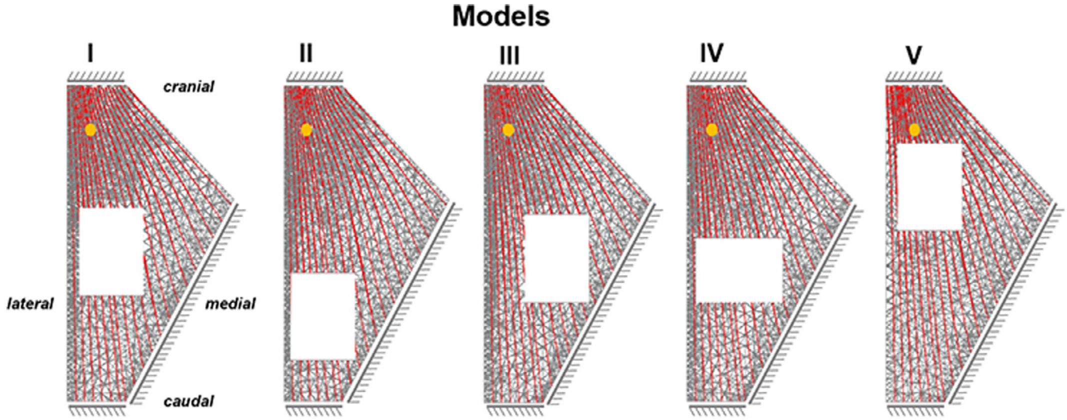

Fig. 2. Five different injuries (11×15 mm^2) were created in the rat LD model at varying locations within the muscle. Red lines across each muscle represent the fiber direction, and the yellow dot represents the thoracodorsal nerve location. First, the injury was placed in the middle of the rectangular portion of the LD (Model I) and then the injury was moved within the anatomical constraints of the muscle. The movement of the injury was limited by the muscle boundary as well as the nerve location. (For interpretation of the references to colour in this figure legend, the reader is referred to the web version of this article.)

Table 2
Animal weight and LD muscle weights.

Group	Animal weight (g)	Excised muscle weight (g)	LD muscle weight (g)
Intact (n = 6)	405.1 ± 29.9	0	1.890 ± 0.234
Experimental I (n = 5)	416.7 ± 30.7	0.282 ± 0.380	1.903 ± 0.112
Experimental V (n = 6)	417.0 ± 34.7	0.122 ± 0.010	1.878 ± 0.220

cranial x-z surface which corresponded to end-to-end fibers and then force production from those specific nodes was measured in AMPS. Model outputs of along-fiber stretch and along-fiber shear strain distributions were assessed at the time of maximum contraction. The normalized fiber lengths within the models were determined by mapping the fiber trajectories from computational fluid dynamics through the FE mesh and then tracking those fibers throughout the simulation to determine their change in length and pennation angle using MATLAB (MathWorks) software (Passipieri et al., 2019).

2.2. Animals

In total, 17 Male Lewis rats (Charles River Laboratories) aged 20 weeks were used for *in situ* analysis. The Institutional Animal Care and Use Committee of the University of Virginia approved all animal procedures.

2.3. In situ testing of the rat LD muscle

2.3.1. Surgical setup

Custom nerve cuffs were made to directly stimulate the thoracodorsal nerve innervating the rat LD (Chen and Walters, 2013). The cuffs consisted of silicone tubing (0.762 mm inner diameter, Dow Corning) and two stainless steel wires (Cooner Wire) running through the tubing. A slit the length of the tube allowed the nerve to be placed inside.

While under isoflurane anesthesia, a 10 cm incision was made from the base of the neck down the spine of the rat and another posterior incision was made the length of the left forelimb. The entire left LD was exposed and the tendon insertion point on the humerus was dissected. The tendon was cut and then pierced once with 3-0 silk suture right above the tendon-muscle insertion so as not to injure the muscle and impact force production. Additional 3-0 silk was knotted around the tendon to adequately secure the suture to the tendon. Approximately 15 mm of thoracodorsal nerve was then carefully dissected from the muscle. The nerve was placed in the nerve cuff and suture was tied around the cuff to keep the nerve in place.

For VML injury groups, the injury was made in the LD prior to cutting the tendon. With the LD exposed, a defect $11 \times 15\ \text{mm}^2$ was excised from the LD muscle in two different locations, both 1–2 mm from the lateral edge of the LD. For Experimental Injury I, the bottom edge was placed 5 mm above the caudal edge of the rib cage. For Experimental Injury V, the top edge was placed 10 mm below the cranial edge of the LD.

2.3.2. In situ measurements

Immediately following surgical setup, *in situ* functional assessment was performed as previously described with modifications using an Aurora muscle lever system (Aurora Scientific, Mod 305C-LR-FP) (Chen and Walters, 2013). Under anesthesia, the rat was placed in the right lateral recumbent position on a heated platform and the tendon suture was connected to the lever arm. The rat was anchored to a metal rod running along the platform by its spine to prevent the rat from shifting during muscle contraction. The nerve was stimulated through the nerve cuff using an Aurora Scientific stimulator (Model 701C). Muscle length was optimized using stimulations at 1 Hz to identify the muscle length with the largest twitch contraction. A stimulation of 1 Hz was used because at higher frequencies, the suture is more likely to rip out of the tendon; therefore, we needed to minimize the number of high frequency stimulations to avoid damage during the experiment. Contractile function of the LD was assessed at the determined optimal length by measuring isometric force at a range of stimulation frequencies to ensure tetanic force was reached (10–200 Hz). After testing, animals were euthanized via CO_2 inhalation and the LD muscle was harvested. Peak isometric force was determined to be the maximum force value achieved at a frequency greater than 100 Hz. Each maximum isometric force value was then normalized to the weight of the muscle to account for biologic variability between animals.

2.4. Statistical analysis

All weights and experimental isometric force values were reported as mean values with standard deviation and compared between groups using a one-way analysis of variance (ANOVA). Force-frequency curves were reported as mean values with standard deviation and compared between groups using a two-way ANOVA. If significant differences were observed in any statistical test, a Holm-Sidak post hoc test was performed. The level of significance was set at $P < 0.05$ in all statistical tests (GraphPad Prism).

3. Results

3.1. Model prediction of injury location effect

Moving the injury location within the boundaries of the muscle demonstrated that a caudal injury (Model II) generates a force value closest to an intact muscle (Fig. 3). An injury in the middle of the muscle (Model I) resulted in generation of 4.1 N of force, 36% lower than intact muscle. Other injuries in the middle region (Models III and IV) generated comparable force values to Model I. The injury location that created the largest force deficit from intact was located cranially (Model V), and this model isometric force prediction was 50% lower than an intact LD.

3.2. Experimental validation of injury location effect

First, the injury location of Model I was created *in vivo* and force production was immediately tested *in situ* (Fig. 4C). The predictions of Model I, 2.6 N/g, were validated by the experimental force values, 2.8 ± 0.3 N/g (Fig. 4A). Then the force predictions of Model V, 2.1 N/g, were tested and confirmed by the experimental results, 2.0 ± 0.2 N/g (Fig. 4A). There was a significant difference in isometric force between all experimental groups. The force-frequency plots in Fig. 4B demonstrate that maximum tetanic force was reached in all groups. Furthermore, at any frequency above 40 Hz, the normalized force of contraction for Experimental Injury V and Experimental Injury I was significantly less than the intact group (Fig. 4B). Animal weights and LD muscle weights remained similar between groups with no significant difference measured (Table 2).

For both Experimental Injury I and V groups, the injury area ($11 \times 15\ \text{mm}^2$) was consistent; however, a smaller muscle weight was excised for Experimental Injury V compared to I. The fibers cranially are under more tension *in vivo*, and thus, when muscle is excised, fibers contract and the defect is larger than originally measured. Therefore, less muscle was excised for Experimental Injury V to create an injury with the same dimensions as Experimental Injury I (upper panels of Fig. 4C show the equivalent size of injuries I and V). When the LD muscles were excised and no longer under tension, the difference in excised muscle tissue volume was again obvious (lower panels of Fig. 4C show the size of Experimental Injury V was clearly smaller than Experimental Injury I).

3.3. Analysis of injury location effect

The mechanisms responsible for the observed difference in force production between the 5 distinct injuries was explored

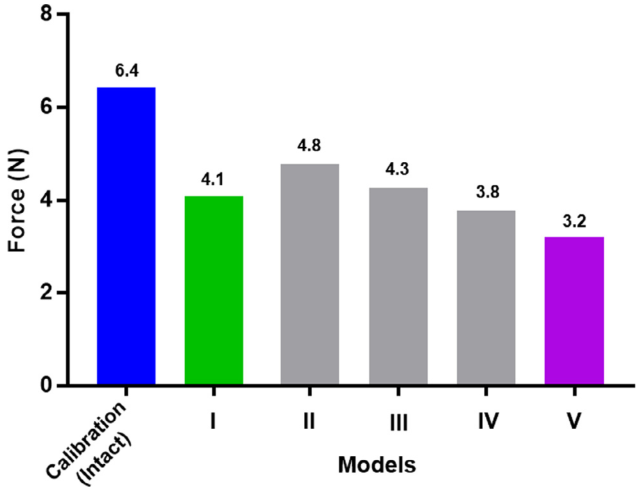

Fig. 3. The injury in the middle of the rectangular portion (Model I) generated 36% less force than the intact muscle. A sensitivity analysis to injury location showed that the model simulated force production of the injury near the cranial boundary of the muscle (Model V) resulted in the smallest force value compared to intact.

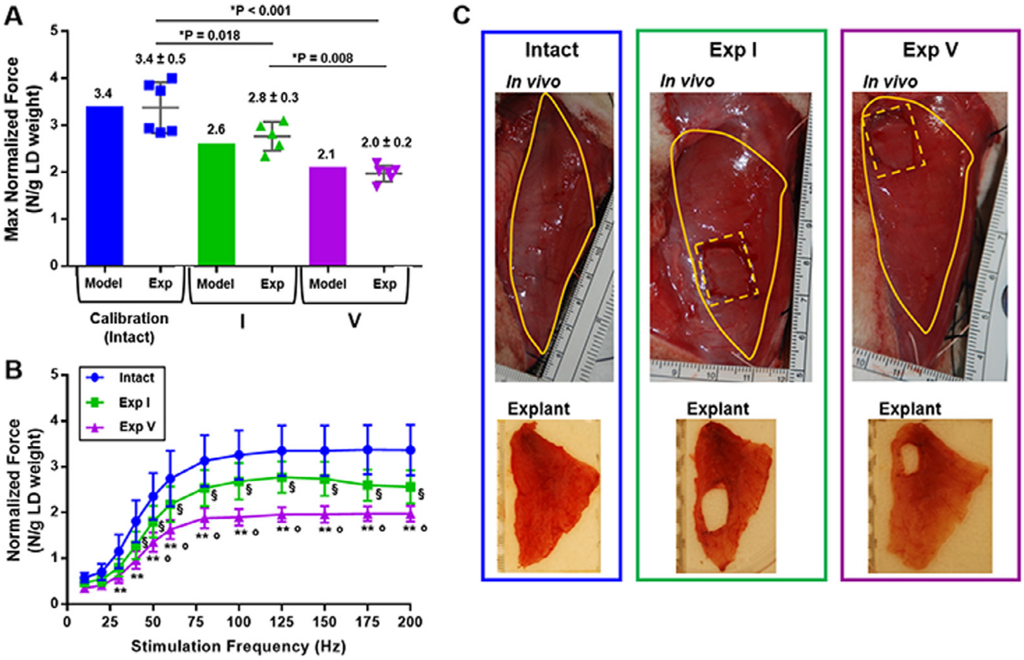

Fig. 4. Results of groups Experimental I (n = 5) and Experimental V (n = 6), shown as scatter dot plots, validate the model normalized force predictions, shown as bars (A). The LD weight normalized force-frequency curves demonstrate that maximum tetanic isometric force was achieved for each group (B). ** indicates statistical significance between intact and Experimental V, ° indicates significance between Experimental I vs Experimental V, and § is for intact compared to Experimental I. Representative images of intact, Experimental I and Experimental V LDs just before testing (*in vivo*) and after harvest (explant) (C). Solid yellow line denotes approximate boundary of LD muscles *in vivo* and dashed yellow boxes mark injury border. (For interpretation of the references to colour in this figure legend, the reader is referred to the web version of this article.)

using the FE LD model. Injury location affects the percent of non-end-to-end fibers attached at the cranial edge of the LD muscle (Fig. 5A). In Model II, for example, the injury is in the most caudal portion of the muscle and 26% of the fibers attached cranially are non-end-to-end. As the injury is moved cranially, the region of non-end-to-end fibers increases and at the most cranial point of injury (Model V), 45% of the fibers are non-end-to-end. The increase in cut fibers contributes to the lower isometric force of the cranial injury location.

The non-end-to-end fibers are not anchored caudally and thus must contribute to force production by laterally transmitting force to end-to-end fibers through the connective tissue (Huijing et al., 1998; Jaspers et al., 1999; Street, 1983). The extent to which non-end-to-end fibers contribute to total muscle force provides a measure of the contribution of lateral force transmission in the muscle, and this non-end-to-end fiber force contribution varied between injuries (Fig. 5A). Model II has the smallest percentage of non-end-to-end fibers and thus those fibers contribute the least to total force compared to other injured muscles (12%). On the other hand, Model V has the largest percent of non-end-to-end fibers; however, these fibers generate less force than end-to-end fibers and the result is a smaller total force.

Lateral force transmission increases in injured compared to intact muscle as highlighted by the along-fiber shear strain distributions of the intact model, Model I and Model V at the time of maximum isometric force (Fig. 5B). During activation of intact and injured muscles, fibers slide past each other causing the connective tissue to deform and experience stress. Therefore, larger shear strains are indicative of larger shear deformations of the connective tissue which physically translates to larger contributions of lateral force transmission (Sharafi and Blemker, 2011). Comparison of the along-fiber shear strains of the models demonstrates that injury location affects the magnitude and distribution of shearing within the muscle compared to intact muscle. Focusing specifically on the triangular portion of the LD, the intact model shows minimal along-fiber shear strain, Model I shows areas with increasing strain, and Model V shows distinct areas of large shear strain.

To better understand the difference in force production between the two injuries tested experimentally, longitudinal force transmission was also explored for Models I and V. The along-fiber stretch distributions at the time of maximum force show regional variability along the muscle length (Fig. 6A and C). To quantify the difference between injuries, normalized fiber length for both regions of non-end-to-end and end-to-end fibers was measured at the point of attachment. In Model I, 33% of the fibers are non-end-to-end and operate low on the ascending limb of the force-length curve and generate minimal isometric force (Fig. 6B and Table 3). In Model V, 45% of the fibers are non-end-to-end and operate very low on the ascending limb of the force-length curve contributing to a total weighted normalized fiber force of 0.488 (Fig. 6D and Table 3). This is lower than the weighted normalized fiber force of Model I, 0.557, and contributes to the lower observed isometric force of the cranial injury location.

4. Discussion

VML injuries are a challenging medical condition to treat because of the variability in wound location, which translates into a wide spectrum of permanent functional deficits. While VML injuries are inadequately treated with current therapeutics, regenerative medicine technologies offer great potential for improved functional outcomes (Baker et al., 2017; Chen and Walters, 2013; Corona et al., 2013). However, more rapid and efficient clinical translation of regenerative therapeutics would likely be aided by a computational tool that can capture the intrinsic variability of VML injuries to first predict anticipated functional outcomes of specific VML injuries, and eventually, to guide injury specific treatment options. Thus, we report the development of a novel coupled framework of *in situ* and *in silico* methods that provides important

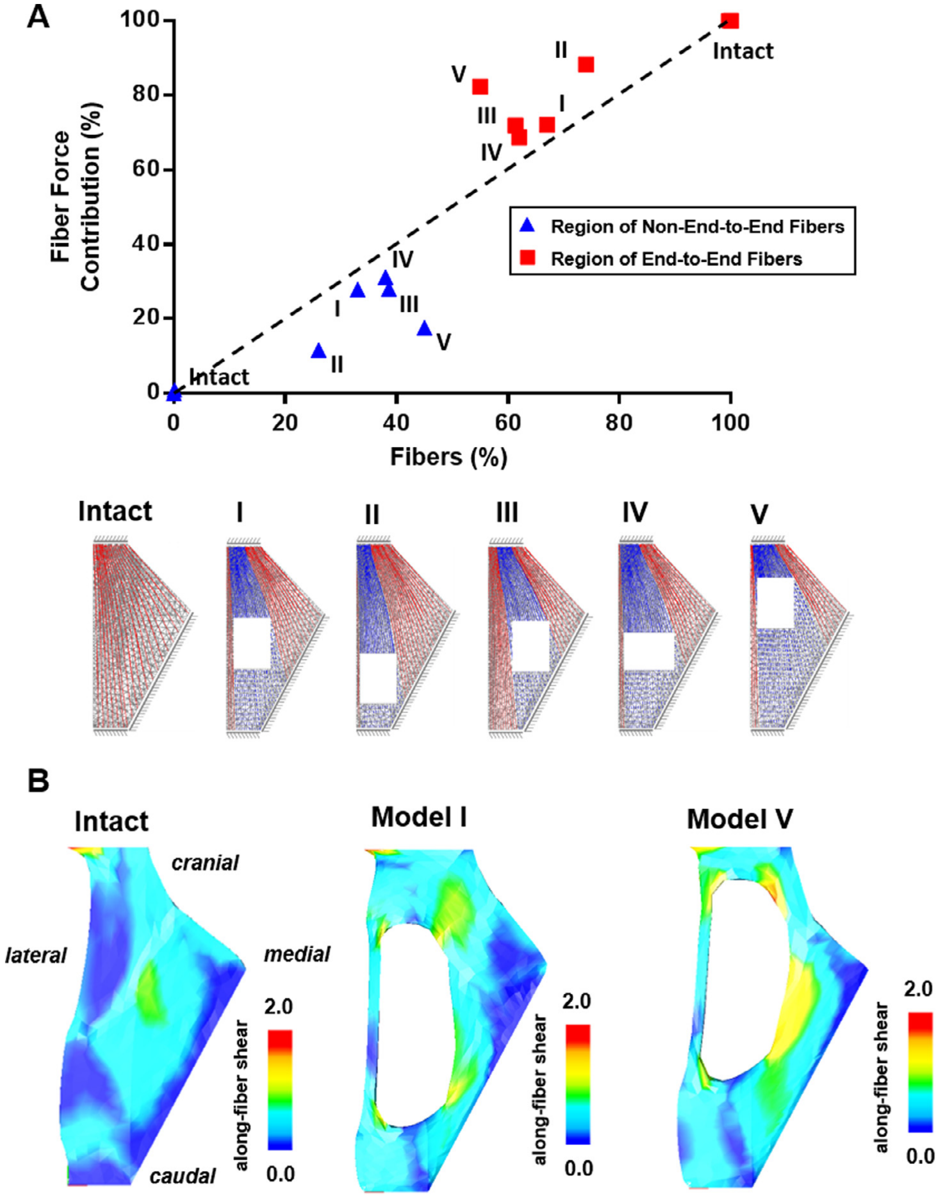

Fig. 5. Injury location affects the percent region of non-end-to-end (blue) and end-to-end fibers (red) present and their respective force contribution (A). The force contribution of the region of non-end-to-end fibers is evidence of lateral force transmission. All fibers in the model are active during the model simulation, and the regional fiber percentages are quantified on the cranial x-z surface of the LD. Along-fiber shear strain distributions of the intact model, Model I and Model V at the time of maximum isometric force provide additional evidence of lateral force transmission and highlight the effect of injury location on shear distributions (B). (For interpretation of the references to colour in this figure legend, the reader is referred to the web version of this article.)

new biomechanical insights regarding the relationship between VML injury location and the corresponding force deficits produced in a clinically relevant rodent LD model.

The use of three different experimental data sets to create (intact data), validate (injury I), and test (injury V) our FE models provides strong confidence in the validity of the model. The predictive force capabilities of the model allowed testing of only two experimental injuries, instead of five, which saved over 90 h of experimental work and approximately 30 rats. Additionally, the force production of Experimental Injury V injury was comparable to another published study which experimentally evaluated a smaller VML injury also near the cranial portion of the rat LD *in situ* (Chen and Walters, 2013).

The experimental and computational coupled framework of this study allows us to explore the relationships between injury location, force production, and the responsible biomechanical mechanisms. The FE model simulations predicted that, for injuries with identical areas, location can have a dramatic effect on force production. Specifically, the cranial injury location (Model/Experiment V) resulted in a functional isometric force deficit 40% below intact values, whereas the same injury area in the middle of the LD (Model/Experiment I) produced a functional deficit only 20% lower than intact values, Fig. 4A.

Interestingly, approximately 6% of the LD weight was removed with Experimental V and about 15% of the LD was removed with Experimental I, yet Experimental V generated 0.8 N/g less force than Experimental I.

Analysis of fiber regions in each injury location model was consistent with the previous experiments that suggest non-end-to-end fibers contribute to force production by laterally transmitting force to end-to-end fibers (Street, 1983). We found that the percent of non-end-to-end fibers increases as an injury location moves cranially, and the percent force contribution of non-end-to-end fibers varied with injury location. Specifically, the percent of injured

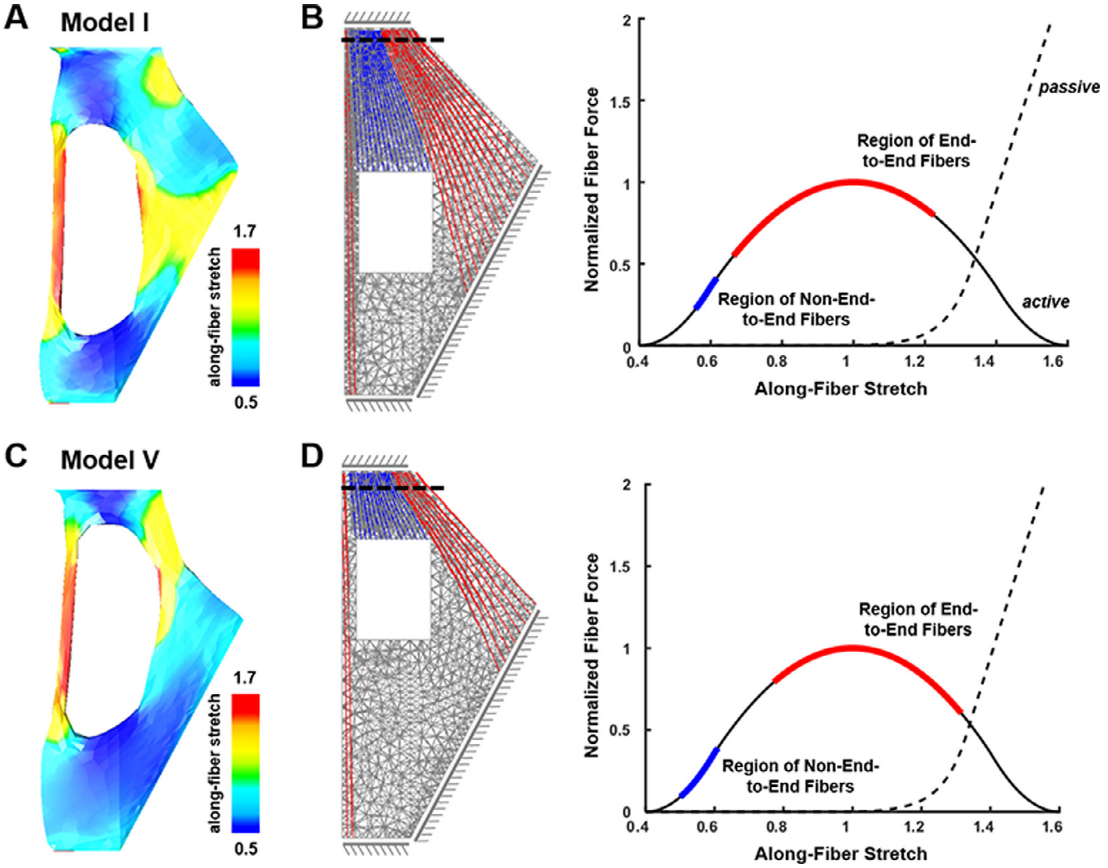

Fig. 6. The along-fiber stretch distribution at the time of maximum force contraction shows regional variations in fiber length for both Model I (A) and Model V (C), where the models assume all fibers start at their optimal fiber length and stretch < 1 for a shortening fiber. Further analysis into fiber length variability measured the normalized fiber length of the region of non-end-to-end (blue) and end-to-end fibers (red) 3 mm from the cranial attachment of the LD (dotted line on LD). In Model I, 67% of the fibers are end-to-end and operate near the optimal length on the force length curve and are capable of generating optimal force production (B). In Model V, 45% of the fibers are non-end-to-end and operate very low on the ascending limb of the force-length curve and account for the low force production of the injured muscle (D). Force-length curves depict the standard deviation range for each fiber region. (For interpretation of the references to colour in this figure legend, the reader is referred to the web version of this article.)

Table 3
The normalized fiber lengths and active forces for end-to-end and non-end-to-end fibers for both Model I and Model V. Fiber lengths and fiber region percentages were measured from model deformations. The normalized fiber force was determined from the active force-length curve using the calculated normalized fiber length. Total normalized fiber force for the muscle was found by weighting the calculated average fiber force by each fiber region percentage.

Group	Fiber Type	Normalized along-fiber stretch	Normalized fiber force	Fiber region percentage	Total weighted normalized fiber force
3 mm from cranial edge of LD					
Model I	End-to-End	0.945 ± 0.280	0.675 ± 0.240	67.0%	0.557
	Non-End-to-End	0.587 ± 0.030	0.317 ± 0.092	33.0%	
Model V	End-to-End	1.04 ± 0.27	0.700 ± 0.250	55.0%	0.488
	Non-End-to-End	0.555 ± 0.055	0.230 ± 0.150	45.0%	

fibers affects how lateral force transmission influences total force production (Fig. 7). Models II and III generate more force than would be predicted if there was no lateral transmission indicating that lateral transmission improves force production. However, comparison of Model V to this idealized scenario indicates that force production is impaired. This may be a result of the large number of injured fibers causing larger deformations, increased shearing, and thus impairing longitudinal force transmission as shown by the increased range of end-to-end fiber lengths and suboptimal normalized fiber force (Fig. 6D and Table 3). Future studies will further explore this complicated relationship between lateral and longitudinal force transmission.

The effects of injury location on force production can further be explained by exploring local variability of fiber lengths along the length of the muscle using the model. The along-fiber stretch, which is fiber length relative to the original optimal fiber length, distributions of Models I and V demonstrate the non-uniformity of fiber length within the LD. The local length variation along the LD is consistent with other studies that have demonstrated that myofiber length varies substantially across entire muscles (Moo et al., 2016; Willems and Huijing, 1994). When the fiber length is measured near the LD's attachment, which is where the force is measured *in situ*, Model V has a larger percent of non-end-to-end fibers operating at a shorter along-fiber stretch than Model I. This larger percentage of shorter fiber lengths likely accounts for the lower force production of Model V compared to Model I.

The demonstrated ability of the LD FE model to accurately predict experimental results and quantify biomechanical mechanisms provides motivation for additional studies using the model as a predictive tool prior to testing of VML injuries *in vivo*. The model can be utilized to explore the relationship between injury size and force deficits, and furthermore, expanded to include the long-term response of VML injuries by incorporating a passive material to represent the filling of the defect with connective tissue

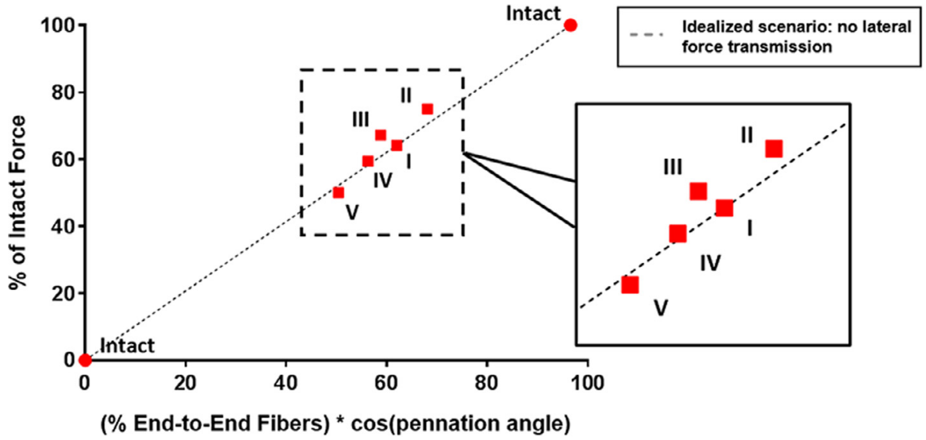

Fig. 7. The relationship between lateral and longitudinal force transmission is affected by the percent of injured/end-to-end fibers. On the x-axis, the percent of end-to-end fibers is multiplied by the cosine of average pennation angle to account for the varying angle of end-to-end fibers in each injury model and allow for direct comparison between models. Each injury cuts different fibers thus altering the average pennation angle and force transmission. The dotted line represents an idealized scenario of no lateral force transmission where the percent of end-to-end fibers directly correlates to force production. Models II and III are above the line indicating that lateral force transmission is contributing to the total force. However, Model V is below the line and lateral force transmission appears to be impairing force production.

or an active material to simulate the regenerative response of a therapeutic. Additionally, the model can be used to identify the preferred experimental injury location in a given muscle to increase the margin of difference between the isometric force produced in intact and VML injured muscles — thus producing more favorable conditions for evaluating treatment effects. Analytic capabilities provided by the model have the potential to significantly increase mechanistic insight, and thus, better inform preclinical experimental design, such as designing a novel therapeutic approach based on the biomechanical requirements of the injury environment.

In conclusion, this work demonstrates that the use of both FE models and *in situ* functional testing of VML injuries provides critical insight into the biomechanical mechanisms governing the relationship between VML injury location and force production/deficit. Combining the tools of the computational modeling and tissue engineering fields should accelerate the development of more efficacious regenerative therapies, and thus, ensure improved functional outcomes following even the most debilitating VML injuries.

Conflict of interest statement

The authors have no conflicts of interest to disclose.

Acknowledgements

Funding for this work was provided by the University of Virginia Orthopedics Research, the Department of Defense (GJ Christ PI, Grants: W81XWH1520012, W81XWH1420004), and the National Science Foundation Graduate Research Fellowship.

References

Baker, H.B., Passipieri, J.A., Siriwardane, M., Ellenburg, M.D., Vadhavkar, M., Bergman, C.R., Saul, J.M., Tomblyn, S., Burnett, L., Christ, G.J., 2017. Cell and growth factor-loaded keratin hydrogels for treatment of volumetric muscle loss in a mouse model. Tissue Eng. Part A 23, 572–584.

Blemker, S.S., Pinsky, P.M., Delp, S.L., 2005. A 3D model of muscle reveals the causes of nonuniform strains in the biceps brachii. J. Biomech. 38, 657–665.

Chen, X.K., Walters, T.J., 2013. Muscle-derived decellularised extracellular matrix improves functional recovery in a rat latissimus dorsi muscle defect model. J. Plast. Reconstruct. Aesthetic Surg. 66, 1750–1758.

Christ, G.J., Siriwardane, M., De Coppi, P., 2015. Engineering muscle tissue for the fetus: getting ready for a strong life. Front. Pharmacol. 6, 1–11.

Corona, B.T., Rivera, J.C., Owens, J.G., Wenke, J.C., Rathbone, C.R., 2015. Volumetric muscle loss leads to permanent disability following extremity trauma. J. Rehabil. Res. Dev. 52.

Corona, B.T., Ward, C.L., Baker, H.B., Walters, T.J., Christ, G.J., 2013. Implantation of in vitro tissue engineered muscle repair constructs and bladder acellular matrices partially restore in vivo skeletal muscle function in a rat model of volumetric muscle loss injury. Tissue Eng. Part A 20, 705–715.

Handsfield, G.G., Bolsterlee, B., Inouye, J.M., Herbert, R.D., Besier, T.F., Fernandez, J. W., 2017. Determining skeletal muscle architecture with Laplacian simulations: a comparison with diffusion tensor imaging. Biomech. Model. Mechanobiol. 16, 1845–1855.

Huijing, P.A., Baan, G.C., Rebel, G.T., 1998. Non-myotendinous force transmission in rat extensor digitorum longus muscle. J. Exp. Biol. 201, 683–691.

Inouye, J., Handsfield, G., Blemker, S., 2015a. Fiber tractography for finite-element modeling of transversely isotropic biological tissues of arbitrary shape using computational fluid dynamics. Simul. Ser. 47, 184–189.

Inouye, J.M., Pelland, K., Lin, K.Y., Borowitz, K.C., Blemker, S.S., 2015b. A computational model of velopharyngeal closure for simulating cleft palate repair. J. Craniofacial Surg. 26, 658–662.

Jaspers, R.T., Brunner, R., Pel, J.J.M., Huijing, P.A., 1999. Acute effects of intramuscular aponeurotomy on rat gastrocnemius medialis: force transmission, muscle force and sarcomere length. J. Biomech. 32, 71–79.

Martins, J.A.C., Pato, M.P.M., Pires, E.B., Jorge, R.M.N., Parente, M., Mascarenhas, T., 2007. Finite element studies of the deformation of the pelvic floor. Ann. N. Y. Acad. Sci. 1101, 316–334.

Moo, E.K., Fortuna, R., Sibole, S.C., Abusara, Z., Herzog, W., 2016. In vivo sarcomere lengths and sarcomere elongations are not uniform across an intact muscle. Front. Physiol. 7, 1–9.

Passipieri, J.A., Baker, H.B., Siriwardane, M., Ellenburg, M.D., Vadhavkar, M., Saul, J. M., Tomblyn, S., Burnett, L., Christ, G.J., 2017. Keratin hydrogel enhances *In Vivo* skeletal muscle function in a rat model of volumetric muscle loss. Tissue Eng. Part A 23, 556–571.

Passipieri J.A.*, Hu X.*, Mintz E.L., Dienes J., Baker H.B., Wallace C.H., Blemker S.S., Christ G.J., In silico and in vivo studies detect functional repair mechanisms in a volumetric muscle loss injury, Accepted Tissue Eng. Part A, 2019. *co-first authorship.

Quarta, M., Cromie, M., Chacon, R., Blonigan, J., Garcia, V., Akimenko, I., Hamer, M., Paine, P., Stok, M., Shrager, J.B., Rando, T.A., 2017. Bioengineered constructs combined with exercise enhance stem cell-mediated treatment of volumetric muscle loss. Nat. Commun. 8.

Rehorn, M.R., Blemker, S.S., 2010. The effects of aponeurosis geometry on strain injury susceptibility explored with a 3D muscle model. J. Biomech. 43, 2574–2581.

Sharafi, B., Blemker, S.S., 2011. A mathematical model of force transmission from intrafascicularly terminating muscle fibers. J. Biomech. 44, 2031–2039.

Street, S.F., 1983. Lateral transmission of tension in frog myofibers: a myofibrillar network and transverse cytoskeletal connections are possible transmitters. J. Cell. Physiol. 114, 346–364.

Willems, M.E.T., Huijing, P.A., 1994. Heterogeneity of mean sarcomere length in different fibres: effects on length range of active force production in rat muscle. Eur. J. Appl. Physiol. 68, 489–496.

Yucesoy, C.A., Koopman, B.H.F.J.M., Baan, G.C., Grootenboer, H.J., Huijing, P.A., 2003. Effects of inter- and extramuscular myofascial force transmission on adjacent synergistic muscles: assessment by experiments and finite-element modeling. J. Biomech. 36, 1797–1811.

Yucesoy, C.A., Koopman, B.H.F.J.M., Huijing, P.A., Grootenboer, H.J., 2002. Three-dimensional finite element modeling of skeletal muscle using a two-domain approach: Linked fiber-matrix mesh model. J. Biomech. 35, 1253–1262.

Zajac, F.E., 1989. Muscle and tendon: properties, models, scaling, and application to biomechanics and motor control. Crit. Rev. Biomed. Eng.